### **SNAME Maritime Convention 2025**

29-31 October 2025, Norfolk, VA Copyright © 2025 Society of Naval Architects and Marine Engineers (SNAME) www.sname.org



# Net drag reduction in high block coefficient ships and vehicles using vortex generators

Jose del Aguila Ferrandis (V)<sup>1</sup>, Jack Kimmeth (SM)<sup>1</sup>, Alfonso Parra Rubio (V)<sup>2</sup>, Neil Gershenfeld (V)<sup>2</sup>, Michael Triantafyllou (M)<sup>1,3</sup>

- 1. MIT Sea Grant, Cambridge, MA
- 2. Center for Bits and Atoms, MIT, Cambridge, MA
- 3. Corresponding Author

We document experimentally at model scale net viscous drag reduction of at least 7.5% in streamlined hulls with high block coefficient, potentially applicable to bulk carriers and tankers, using wedge shaped vortex generators (VGs). We also establish scaling laws proving that at full-scale drag reduction is fully preserved, and estimate the size and cost of VG installation and the gains that can be materialized in ship operations.

KEY WORDS: Hydrodynamics (hull form), Resistance, Fluid-Structure Interaction, Weather Routing

#### INTRODUCTION

The International Maritime Organization (IMO) has set strict carbon emission reduction goals for the shipping industry. By 2050, IMO requires net zero greenhouse gas emissions and has goals for at least a 20% reduction by 2030, and 70% by 2040. To reach these ambitious goals, short, medium, and long-term solutions must be utilized. Ultimately, a transition in prime movers and fuel type will be required to reach 100% greenhouse gas emission reduction, but in the short and medium term, means for reducing drag and improving hull efficiency will enable achieving the 2030 and 2040 goals, and will make the 2050 goal more easily attainable. With this goal in mind, we investigated the use of Vortex Generators (VGs) to reduce the viscous resistance of high block coefficient ships. For example, fuller shaped ships such as bulk carriers and tankers that have block coefficients up to 0.85 (the block coefficient is the ratio of the volume of the ship divided by the volume of the "box" that contains it, viz. the product of the length, beam, and draft), although streamlined with high length to-beam ratios, can have pressure drag that is up to 35% of the viscous drag, or even higher. We utilized a combination of experimental testing and computational fluid dynamics simulations, assisted by optimization methods, to investigate different geometries for the vortex generators and found that the optimal shape was a wedge shaped vortex generator; we then ran several different designs in the MIT Towing Tank on an axisymmetric model to find the optimal vortex generator design for a given speed. Appendix A contains design dimensions of the wedge VGs.

The net drag on streamlined bodies in high Reynolds number flow is comprised of viscous and added drag components. Viscous drag is comprised of both frictional and form drag, whereas added drag encompasses more case-specific components such as wave resistance, and added resistance in storms for surface vessels. Frictional drag tends to dominate the viscous drag in more streamlined bodies, but in geometries with high block coefficient, form drag is significant.

Vortex Generators aim to reduce form (pressure) drag induced by boundary layer separation by drawing high momentum fluid into the boundary layer, delaying separation and reducing pressure drag, and potentially even offsetting the parasitic drag induced by the addition of VGs.

There have been some successful efforts to reduce separation drag in specific applications, including the flow around bluff bodies and the flow around wings at large angle of attack. Studies in bluff bodies, for which pressure drag constitutes more than 90% of the total drag at high Reynolds numbers, have demonstrated large reductions in drag through control of flow separation. An example that is often quoted in fluid mechanics textbooks is the incorporation of dimples in moving golf balls under laminar flow conditions, to force the boundary layer to become turbulent and hence separate further downstream along the surface of the golf ball, reducing the wake width and hence the pressure drag (Bearman 1976, and Chowdhury et al. 2016). Although effective in reducing drag in spheres that move at speeds corresponding to laminar boundary layer flow around the sphere, but at Reynolds numbers close to transition to turbulence, such methods have been applied successfully to bluff bodies only (Achenbach 1972).

In aerospace engineering, controlling the boundary layer using vortex generators (VGs) (Babinsky and Harvey 2011) is being used in wings to maintain aerodynamic lift at higher angles of attack (Gad-el 2000) and delay stalling. The main focus here is to prevent loss of lift, which can occur due to flow separation (Milton and Smith 1956), once a threshold angle of attack is exceeded. Vortex generators are strategically placed to produce small, streamwise vortices that energize the boundary layer (Gad-el 2000, Lin 2002), which adheres to the wing surface for longer distances, effectively delaying stall. This technique is particularly beneficial under angles of attack leading to stalled conditions (Lin et al 1990), where the flow over the wing resembles that around bluff bodies, as it separates along distinct separation lines.

Vehicles in the marine and aerospace industry have a hull that is generally well streamlined, viz. they have elongated bodies, with high length to transverse dimension ratios, and smooth curvatures at the front and rear parts of the hull. In marine vehicles the focus is on minimizing drag on elongated hydrodynamic bodies like ship hulls and underwater vehicle hulls, while there are generally no lift considerations, except in few, specialized cases such as airfoil-supported craft. Many commercial ships, although slender, have a fuller shape, in order to carry more cargo; hence, a major target can be to reduce the pressure drag that develops in the afterbody.

As mentioned, a passive means for reducing separation are vortex generators. However, to achieve overall drag reduction, it is also required that the drag caused by the VGs themselves be sufficiently small. Hence the focus in this study is to consider the type of vortex generators that reduce separation through re-energizing the boundary layer and yet have small parasitic drag.

### OPTIMIZATION OF VORTEX GENERATORS

We document experimentally at model scale net drag reduction using Vortex Generators (VGs), optimized first 2 2025 SNAME Maritime Convention Page 2 of 17 through the use of systematic CFD driven by Gaussian Process Regression, and then running a sequence of experimental runs on hulls equipped with VGs. We used a submerged body since we had to test at much higher speeds than Froude scaling would dictate, in order to achieve supercritical Reynolds numbers. This had the added benefit that there was no wave resistance at model scale and we could directly assess viscous drag reduction. We opted for an axisymmetric hull for convenience of construction since we had to fabricate multiple hulls in order to parametrically test and optimize the VGs.

We also performed a study on how these results would translate in full-scale ships. First, we show that the percent reduction in form drag will be roughly the same in full scale as in model scale. Next, we used some realistic assumptions to translate the results from an axisymmetric hull to a ship hull: We consider the axisymmetric body roughly equivalent to a double hull. Although in a ship the curvature in the stern is three-

dimensional, we consider the curvature in the streamwise direction as the primary component driving form drag; hence matching that component of curvature between model and ship we expect similar values of form drag coefficient. We account for differences in the relative boundary layer thickness and the number of VGs needed (at full scale, more VGs of smaller relative size are needed than at model scale). The purpose of the study is to provide reasonable estimates rather than precise numbers, which would require a much more extensive testing procedure than that which the authors had resources to undertake. Considering the effects of including the other components of the resistance as well as the route statistics on the expected drag reduction was done to place in context the final drag reduction gains.

### **Computational Analysis**

Initial investigation into the utilization of vortex generation to induce a drag reduction in hydrodynamics began with a computational fluid dynamic (CFD) analysis. Also, models of an axisymmetric hull with (a) a smooth tail, (b) a tail with delta wing vortex generators, and (c) a tail with wedge vortex generators were produced and tested experimentally.

We employed Detached Eddy Simulation (DES) to evaluate and compare different VG designs. We consider this analysis to be qualitative, as there are modeling limitations by this method, such as considering boundary layers in adverse pressure gradients, as well as with the resolution of turbulent eddies within the boundary layer.

DES represents a computational approach that combines Unsteady Reynolds-Averaged Navier-Stokes (URANS) with Large Eddy Simulation (LES) to simulate turbulent flows characterized by both attached and detached eddies. This hybrid approach is efficient and cost effective to investigate the complex interactions between flow fields and vortex generators (VGs). Although they offer the possibility to directly resolve boundary layers following URANS equations, the turbulence models that are used to provide closure are empirically calibrated and are only fully valid in the absence of adverse pressure gradients. Furthermore, the averaging of viscosity effects and, by extension, of the turbulent eddy structures represent a less perturbed flow than in the experiments. DES leverages the Navier-Stokes equations, tailored for either URANS or LES modes depending on the flow region. In areas close to the body surface, DES employs URANS equations, utilizing the SST-Menter k-omega model to predict turbulent properties of the flow. The effective3 Page 3 of 17 2025 SNAME Maritime Convention ness of this model in capturing boundary layer phenomena makes it a good candidate for VG analysis. Compromises, however, are made in the modeling of the boundary layer: Although our meshes are fully resolved and use no wall functions, the equations resolved are URANS with SST-Menter k-omega model.

$$\frac{\partial \bar{u}_i}{\partial t} + \bar{u}_j \frac{\partial \bar{u}_i}{\partial x_j} = -\frac{1}{\rho} \frac{\partial \bar{p}}{\partial x_i} + \nu \frac{\partial^2 \bar{u}_i}{\partial x_i \partial x_j} - \frac{\partial \overline{u_i' u_j'}}{\partial x_j} (1)$$

Equation 1 is the URANS equation, which uses Menter Shear Stress Transport (SST) k- $\omega$  turbulence modeling to resolve the added unknowns the  $\partial u$  ' iu ' j term introduces. While the DES approach captures boundary layer phenomena well, there are notable caveats that come with it. Namely, DES has computational demands that are notably less than LES, but, still, for the complex geometries being investigated they are demanding in terms of computational time. Also, accuracy is highly sensitive to grid resolution, which necessitates intensive model meshing to capture data at the transition from RANS to LES. Finally, there are overall limitations in the model's ability to accurately capture turbulent flow; the most notable discrepancy observed being the actual point of flow separation observed in model testing and the point predicted by DES.

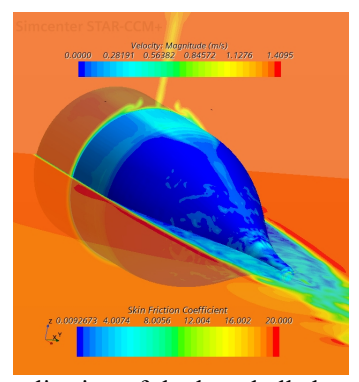


Fig. 1: Flow visualization of the bare hull shows very low skin frictional coefficient, reflecting detached flow; the wake contains unsteady patterns, as seen in the horizontal cut provided along the centerline, negatively impacting the performance of a propeller placed at the stern of the vehicle.

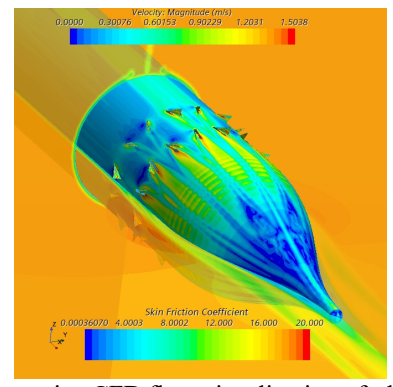


Fig. 2: Representative CFD flow visualization of a hull with deltalike VGs exhibits a nearly attached flow to the trailing edge and smooth velocity distribution, but with increased skin friction coefficient.

Net drag reduction in high block coefficient ships and vehicles using vortex generators

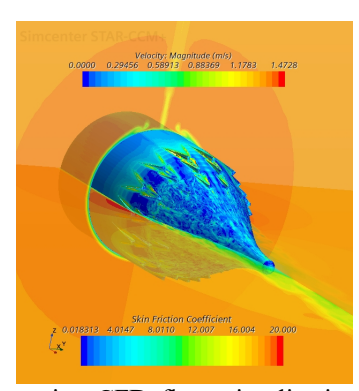


Fig. 3: Representative CFD flow visualization of a hull with wedge VGs shows an attached flow almost to the trailing edge, combined with low skin frictional coefficient, indicating good performance of the VGs.

Figures 1, 2, and 3 represent the results of optimization of the tails equipped with (a) delta-like VGs (figure 2) and (b) wedge VGs (figure 3) compared with the bare hull of figure 1; investigated using DES. Both sets of VGs cause the boundary layer to reattach but the most notable difference between the delta wing VGs and the wedge VGs is in the skin frictional coefficients (Cf). The delta winglet VGs visually exhibit similar boundary layer flow reattachment at the stern to the wedge VGs but with higher skin Cf. This difference indicates that the wedge VGs have better performance than the delta wing VGs.

### **Experimental Investigation**

Experiments were conducted in the MIT tow tank with both deltawing vortex generators and wedge vortex generators, using a first design of the axisymmetric hull of length 1.2 m, in 2023 (figure 5). The data acquisition system comprised a load cell amplifier and an NI USB-6218 DAQ board for force measurement. A computer running LabVIEW software was utilized for real-time data recording, enabling detailed analysis of the hydrodynamic forces. The model used was designed to match the maximum curvature of a high block coefficient (Cb) bulk carrier. We used Hama strips (Hama et al 1957) at the nose of the vehicle, to ensure a turbulent boundary layer over most of the surface of the body. The tests included dye flow visualization which validated the CFD simulations (figure 4).

In this set of tests we ran the model at speeds from 0.5 to 1.3 m/s, using multiple versions of the delta wings with varying dimensions and number of rows of VGs, in order to find an optimal configuration. Only two variations of the delta VG shape were used in this set of experiments, comprising a longer and a shorter VG model.

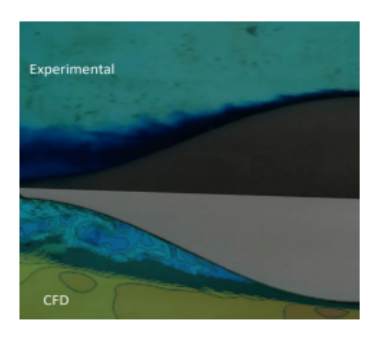


Fig. 4: Experimental Flow Visualization using dye, compared to CFD flow visualization at a speed of 1.3 m/s.

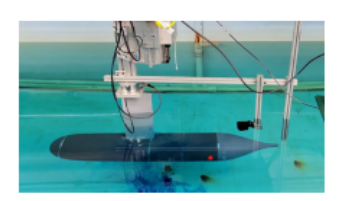


Fig. 5: Initial Experimental set up, showing the submerged axisymmetric model rigidly attached at about mid-length to the towing carriage through a streamlined strut.

The net drag observed by a force sensor was recorded and compared to the bare tail drag. While the dye flow visualization showed a flow similar to the flow in CFD (figure 4), confirming delayed flow separation, this iteration of tails showed higher total drag than for the bare tail, for all versions used (Figure 6), because of the high parasitic drag of the VGs.

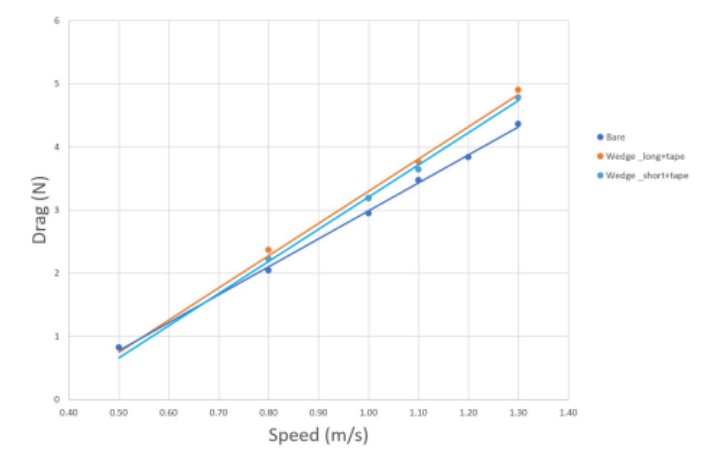


Fig. 6: Drag of hull with (a) Delta VGs (upper curve), (b) wedge VGs (middle curve), and bare hull (lower curve).

Given that the short wedge VGs were found to perform better than the delta VGs in both the CFD analysis and the first iteration of experiments, moving forward only wedge VGs were investigated as possible boundary layer reattachment devices. The next set of experiments focused on varying the location, height, and overall size of the wedge VGs to maximize the net drag reduction, accounting for the parasitic drag incurred by adding the VGs.

These tests were conducted at 1.3 m/s first with a bare tail and then with the three versions of the wedge VGs. Tests conducted at 1.3 m/s were deemed most representative because the Reynolds number is sufficiently high (Re  $\approx 1.6 \times 10^6$ ) so that with the Hama strips the flow is turbulent over most of the surface

Net drag reduction in high block coefficient ships and vehicles using vortex generators

of the model; for higher speeds the time window of collecting data in the 35 meter MIT tank becomes shorter as speed increases and reliability of force measurements decreases.

The Hama strips were adjusted until the drag we measured was that of a body with fully turbulent flow at the corresponding Reynolds number. Indeed, for U=1.3 m/s the ITTC curve provides cf =  $4.25\times10{-}3$  while we measured cD =  $6.83\times10{-}3$ . Accounting for front end effects and the strut-hull interaction (the strut drag was measured separately and subtracted from the measurements), this gives a form factor 1+k=1.4.

It should be noted that this form factor is close to the form factor for the 300 m long bulk carrier we use in a later section, estimated as k=0.37 using the empirical relations in Holtrop-Mennen (1982). The stern form of this bulk carrier and, in particular, its maximum streamwise curvature was used to design the stern section of the axisymmetric model to have a similar curvature value.

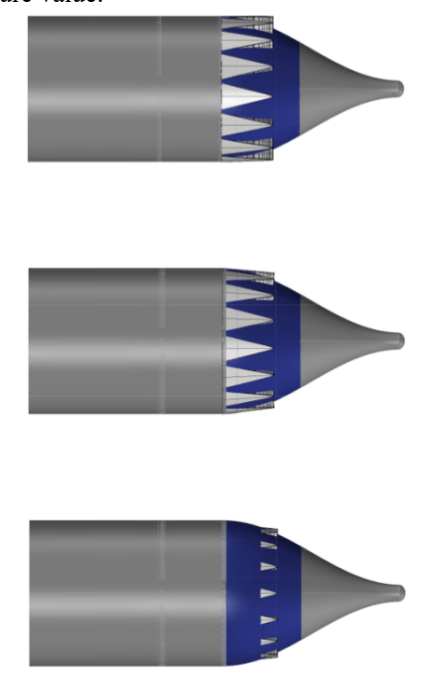


Fig. 7: CAD Models of experimental tails Tail 1, Tail 2, & Tail 3 (Descending Order).

The bare tail running at a speed of 1.3 m/s had an average drag of 4.444 N. The first of the three experimental tails tested (see figure 7) provided an average drag of 4.587 N, viz. higher than for the bare tail. Tails 2 and 3 were designed with recesses to reduce the VG surface and, also, varied the exposed height to reduce the added parasitic drag. Tail 2 has a height of 9.0 mm and Tail 3 has a height of 7.0 mm. Tail 2 had an average drag of 4.357 N, which provides a 1.96% reduction. Tail 3 had an average drag of 4.108 N, which provides a 7.56% reduction and was adapted as the standard tail from then on.

Flow visualization was also conducted in this set of tests using tell tails attached at to the stern of the model. As seen in figure 8, the tell tails show a more uniform flow for all versions of the VGs used, characteristic of attached flow; while the tell tails for the bare tail show a separated flow.

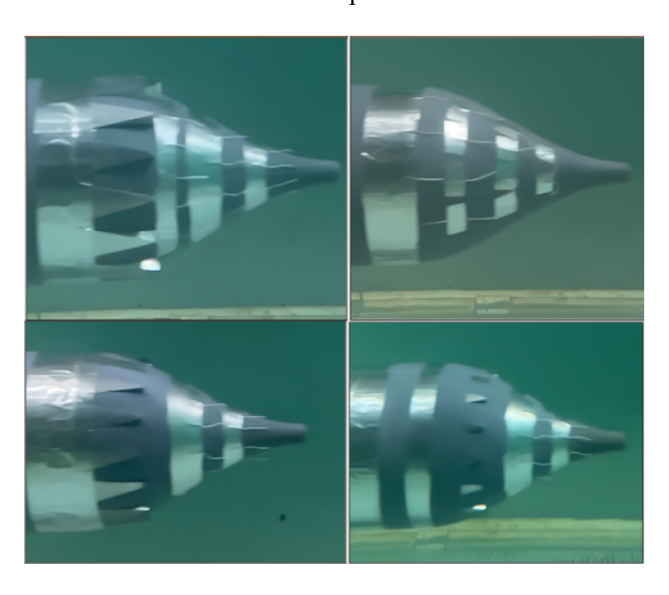


Fig. 8: Tell Tail Comparison, tail 1 top left, bare tail top right, tail 2 bottom left, tail 3 bottom right. The last row of tell tails shows turbulent flow in the bare tail test runs and uniform reattached flow in the other tails.

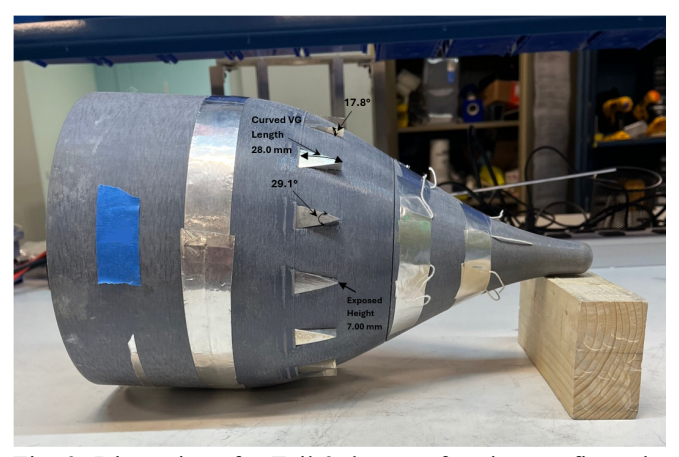


Fig. 9: Dimensions for Tail 3, best performing configuration in terms of drag reduction. See Appendix for tabulated values.

# Finalized set of experimental tests

In the last set of tests, the range of 1.0 m/s to 1.6 m/s was used to test both the bare tail and the best performing tail 3 (figure 9). The apparatus in the Towing Tank was reinforced for stable towing and experiments were conducted with the new model, so some small deviations from previous experiments were expected. Each tail was run within this speed range ten times for each velocity and the average drag and standard deviation were calculated. As

Net drag reduction in high block coefficient ships and vehicles using vortex generators

shown in figure 10 and in table 1, the tail with wedge VGs performed better at all speeds than the bare tail.

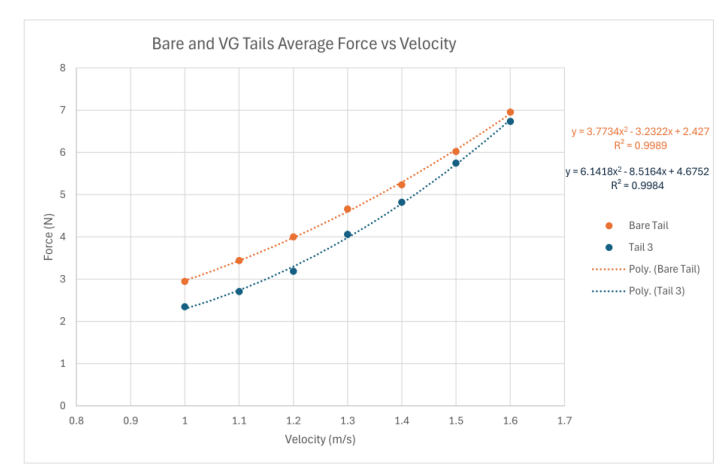


Fig. 10: Drag force as function of speed for a bare hull (red) and a hull fitted with Tail 3 (blue)

Figure 10 depicts the average drag force experienced at speeds from 1.0 to 1.6 m/s. As speed increases, the boundary layer thickness decreases and the relative size of the VGs increases, causing the parasitic drag to increase as VGs protrude further, causing a drop in the net drag savings. We find that for the design speed of up to 1.4 m/s it is safe to assume at least a drag decrease of 7.9%, higher for proper sizing of the VGs.

Table 1: Comparison of Tail 3 and Bare Tail total drag force at varied speeds.

Speed	Tail 3 (N)	Bare Tail (N)	Difference (N)	% Difference
1.0	2.350	2.948	0.598	20.3%
1.1	2.736	3.408	0.672	19.7%
1.2	3.217	3.949	0.732	18.5%
1.3	4.059	4.664	0.605	13.0%
1.4	4.819	5.233	0.414	7.9%
1.5	5.750	6.022	0.272	4.5%
1.6	6.732	6.959	0.226	3.3%

For the present design, the height of the VGs is about 30% of the thickness of the boundary layer at a speed of 1.4 m/s. It is intriguing that for smaller speeds, when the boundary layer is thicker, even larger drag reduction is observed. We are investigating these results for robustness against marine growth, effects from ship motions, etc. For this reason, we target the design at 1.3 to 1.4 m/s with a VG height in the expected range of 25 to 30 % of the thickness of the boundary layer.

# SCALING TO FULL SIZE AND COST ESTIMATION

Next, we proceed with scaling the model test results to a full-scale vessel. Form drag reduction is most effective for vessels with a high block coefficient, like bulk carriers and tankers,

SMC 2025, 29-31 October 2025, Norfolk, VA 5

because they experience significant pressure drag. Since we conducted the tests in a submerged model, we do not apply Froude scaling and, instead, we can use much higher speeds to ensure sufficiently high Reynolds Number (Re).

As an example, we consider a typical large bulk carrier with length L=299.95 m, breadth B=50 m, design draft T=16.1 m, design speed U=14.5 knots, displaced volume 199,755  $\mathrm{m}^3$ , and a 4-bladed propeller with diameter 9.6 m. Two example routes were investigated to calculate the added resistance caused by seastate conditions along these routes at various times of the year.

It should be noted that this calculation should be considered an approximation, since the hull details between the axisymmetric model and the ship are different. The basic assumption is that the maximum hull curvature near the stern along the flow direction is the primary driver for generating form drag in fuller hulls. As a result, we ensured the same maximum curvature in model scale and used the bulk carrier stern outline (on average) to design the model stern outline.

### **Scaling Factors**

To apply these findings to a full-scale ship, we employ a linear scale,  $\lambda$ , representing the ratio of the length of the full-scale vessel ( $L_s$ ) to the length of the model ( $L_m$ ), and a separate scaling factor for the speed,  $\lambda_U$ , equal to the ratio of the full scale to model speeds.

As explained in Appendix A, the dimensions of the ship hull scale as  $\lambda$ , while the VG dimensions scale according to the thickness of the boundary layer  $\delta$ . Likewise, the area of the VGs scales as the square of delta, etc. As a result, the VGs in full scale are smaller in proportion to the ship length than at model scale, while more VGs are required overall, in order to keep the relative distance between adjacent VGs in proportion to the model VGs.

We use the scaling analysis of Appendix A and two assumptions:

- 1. The resistance of the VGs is primarily caused by vortex formation, hence the drag coefficient is roughly the same between model and full-scale vessels. This is a conservative assumption, because the frictional component of the VG drag coefficient decreases with Reynolds number, so the full-scale VGs will be slightly smaller.
- 2. The form drag factor k is the same for the full scale and model scale vessels, a standard assumption in model testing. Likewise, the ship drag reduction (without factoring in the parasitic drag of the VGs), as percent of the overall viscous drag, remains the same at full scale, another standard assumption for form drag, which is caused by the sharp curvature at the stern.

After some analysis, the principal conclusion of Appendix A is that the net viscous drag reduction as percent of the overall viscous drag is the same for the full-scale ship as in model scale. For the example of a 300 m long ship considered,

Net drag reduction in high block coefficient ships and vehicles using vortex generators

the VGs have height 0.356 m, and length 1.424 m, while a total of 31 VGs are required.

# Cost Estimate for installing wedge VGs on a 300 m long vessel

Given the dimensions of the VGs, the volume per VG is 0.766m³, resulting in a total volume for 31 VGs of 23.7m³. Using the American Bureau of Shipping (ABS) Part 5A and 5B, Common Structural Rules for Bulk Carriers and Oil Tankers, providing material grades and mechanical properties for steel construction, we estimate the cost of construction using AH36 steel at between \$130K and \$150K. Using standard assumptions for the cost of welding and painting we arrive at a cost of \$100K to \$115K (Kimmeth 2025).

# EFFECT OF ROUTE STORMS ON DRAG REDUCTION

For the example case of a 300 m long vessel, an analysis of two routes was conducted to determine the effect of the other components of resistance, especially added resistance, on the expected drag reduction and cost savings.

# **Effect of the Selected Route on Net Drag Reduction**

Two specific routes were analyzed to estimate added resistance due to sea state conditions along those routes. These routes are Qingdao port in China (CNQQDG) to Port Headland in Austalia (AUPHE), and a transpacific route from Manzanillo Mexico (MXZLO) to Shanghai China (CNSHA). For these routes ample amounts of data are available for the sea states by season. The second route was chosen to assess the significance of traveling on open ocean rather than the relatively sheltered conditions of the first route.

# **Sea State Analysis**

A 3D CAD model of the selected 300 m bulk carrier was used with the program MAXSURF using the original line plans of the vessel, providing the data shown in the table below.

To analyze the effect of sea state conditions, the still water baseline resistance is obtained and then added resistance is calculated for each specific sea state. Data collection for the routes came from the European Center for Medium-Range Weather Forecasts (ECMWF). ECMWF and the Copernicus Marine Environment Monitoring Service (CMEMS) collaborated to produce sea state data sets, known as the ERA5. ERA5 has been collecting weather information for every hour every day from January 1940 to the present day and has over 100 collection data points, including significant wave height with a resolution of 0.5 degrees of latitude for 0.5 degrees of longitude. This is approximately a 56 km by 56 km grid.

Table 2: Ship Hydrostatic and Stability Parameters

Parameter	Value	Units
Displacement	204043	t
Volume (displaced)	199065.927	m <sup>3</sup>
Draft Amidships	16.100	m
WL Length	299.645	m
Beam max extents on WL	50.084	m
Wetted Area	24694.261	m <sup>2</sup>
Max sect. area	803.094	m <sup>2</sup>
Waterpl. Area	13704.213	m <sup>2</sup>
Prismatic coeff. (Cp)	0.827	_
Block coeff. (Cb)	0.824	_
Max Sect. area coeff. (Cm)	0.997	_
Waterpl. area coeff. (Cwp)	0.913	_
LCB length	154.079	from zero pt. (+ve fwd) m
LCF length	143.550	from zero pt. (+ve fwd) m
LCB %	51.421	from zero pt. (+ve fwd) % Lwl
LCF %	47.907	from zero pt. (+ve fwd) % Lwl
KB	8.386	m
BMt	13.121	m
BML	443.219	m
GMt corrected	21.507	m
GML	451.605	m
KMt	21.507	m
KML	451.605	m
Immersion (TPc)	140.468	tonne/cm
MTc	3129.983	tonne-m
RM at $1^{\circ} = GMt \cdot Disp \cdot sin(1)$	76587.837	tonne-m

This data is analyzed using a MATLAB script to return the Average Wave Height per month for the range of 2011 to 2021. Now that SWH can be found with a 56 by 56 km2 resolution, the specific GPS positions of the routes must be defined. Mock navigational plans were drafted by following the International Maritime Organization's Convention on the International Regulations for Preventing Collisions at Sea (COLREGs), maritime shipping lanes, and distance optimization using app.searoutes.com. 140 waypoint markers along this route were then defined. These waypoints positions were recorded in a GPX file format that can be imported into Matlab for analysis.

The Matlab script then runs calculations for each month separately and returns a percentile distribution of wave heights along the defined route. Shown in table 3.

Table 3: Monthly Analysis of Sea State Probability Along Qingdao to Headland

Month	Sea State 1	Sea State 2	Sea State 3	Sea State 4	Sea State 5
January	0.000	0.110	0.500	0.380	0.000
February	0.000	0.120	0.480	0.400	0.000
March	0.000	0.110	0.500	0.390	0.000
April	0.000	0.120	0.520	0.360	0.000
May	0.000	0.110	0.520	0.370	0.000
June	0.000	0.120	0.470	0.410	0.000
July	0.000	0.120	0.520	0.360	0.000
August	0.000	0.120	0.520	0.350	0.000
September	0.000	0.120	0.500	0.380	0.000
October	0.000	0.110	0.520	0.360	0.000
November	0.000	0.120	0.520	0.360	0.000
December	0.000	0.090	0.430	0.400	0.090

Net drag reduction in high block coefficient ships and vehicles using vortex generators

Once the monthly probability of the sea state has been determined using ERA5 and MATLAB, the added resistance can be calculated utilizing a separate MATLAB script. A polar distribution plot is generated for the added resistance, as function of the relative heading and the sea state condition is generated for each speed. Along with these polar plots, the MATLAB script also provides a summary of the total added resistance due to waves depending on the sea state.

With the known added resistance per sea state and the known sea state probabilities for any given month, added resistance can be calculated for the voyage per month of travel. Figure 11 represents the added resistance that would have been expected by the bulk carrier along this route over the total period of observation, January 2011 to January 2021.

As another case study, the Manzanillo to Shanghai route, was selected for comparison with the relatively sheltered Qingdoa to Headland route. The same process was conducted where the route was determined per COLREGs, shipping lanes and distance optimization.

Table 4: Added Resistance along Qingdao to Headland Route

Sea state	Wave height (m)	Added resistance kN
1	0-0.1	0
2	0.1-0.5	4
3	0.5-1.25	66
4	1.25-2.5	304
5	2.5-3	614
6	4-6	1831

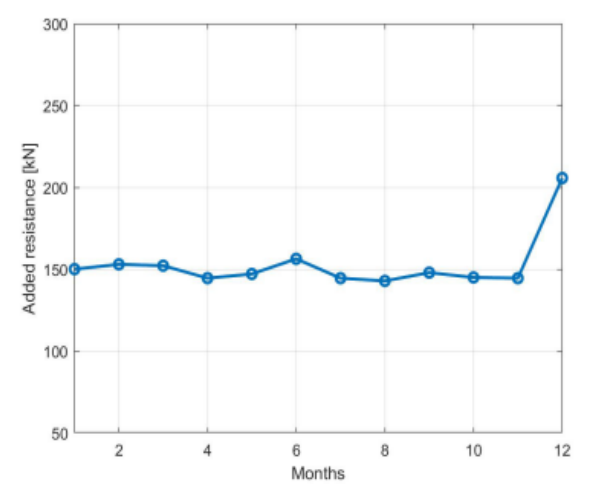


Fig. 11: Added Resistance Annual Qingdao to Headland

The most significant difference between the two case studies was that the discretized way points were evenly spaced at 50 nautical mile intervals resulting in 139 waypoints. These waypoints, the sea state probability, and the relative heading of

the vessel are then used to generate the added resistance curve as function of time over a year (figures 11 and 12).

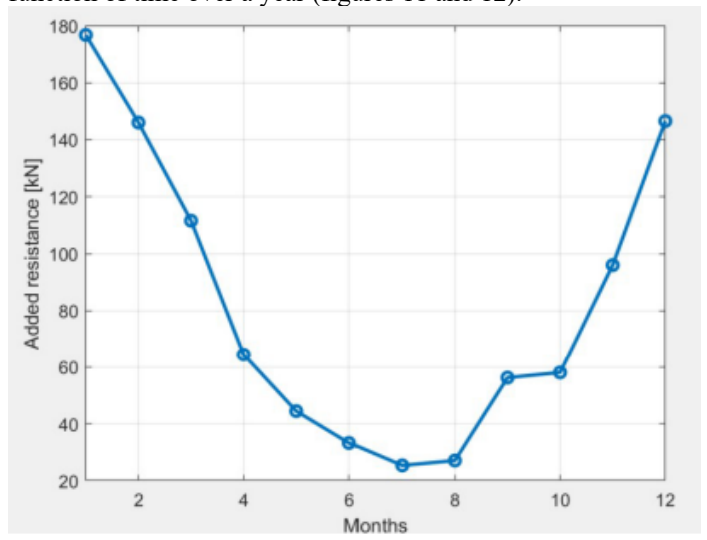


Fig. 12: Added Resistance Annual Manzanillo to Shanghai

### **Drag Reduction in a Sea Route**

Utilizing the ship's hydrostatic principal dimensions and CAD hull model, the model towtank test results can be contextualized. To apply the drag reduction ratio to the overall resistance, the total still water resistance must be broken into components, and the added resistance along the route based on sea state conditions must also be considered. The Holtrop-Mennen method of estimating the resistance for high block coefficient ships allows for a more realistic net resistance reduction to be approximated (Holtrop-Mennen 1982):

$$R_{\text{Total}} = R_F (1+k) + R_W + R_B + R_{TR} + R_A$$
 (2)

Total resistance ( $R_{Total}$ ) has been subdived into:  $R_F$  which is the frictional resistance according to ITTC-1957 friction formula, k is the form factor that describes the form resistance of the hull in relation to  $R_F$ ,  $R_W$  which is the wave-making resistance,  $R_B$  which is an additional pressure resistance due to bulbous bows, and  $R_A$  which is a model-ship correlation resistance.

Using the empirical relations in Holtrop-Mennen (1982) we estimate the form drag coefficient k=0.37, which is reasonably close to the form drag k=0.4, measured experimentally in the axisymmetric model, confirming the hypothesis that the maximum curvature in the stern along the streamwise direction is the major driver of form drag.

The vortex generators target viscous resistance due to boundary layer separation, which is encompassed by R<sub>F</sub> and the form factor, so it is important to have an accurate estimation of these terms. Equations for the corresponding quantities are provided in (Holtrop-Mennen 1982).

Net drag reduction in high block coefficient ships and vehicles using vortex generators

Using the hydrostatic and geometric dimensions attained from MAXSURF and the Holtrop-Mennen method, the Total Still Water Resistance can now be approximated at any given speed. To validate the Holtrop Mennen approximation, R<sub>Total</sub> was compared to the total resistance obtained from sea trials using the measured torque and speed in the trials and estimating the propulsive efficiency (Table 5).

Table 5: Resistance Breakdown in Still Water

U (kts)	$\mathbf{R}_f$ (kN)	$\mathbf{R}_w$ (kN)	$\mathbf{R}_A$ (kN)	$\mathbf{R}_{TR}$ (kN)	R <sub>total</sub> (kN)	$\mathbf{R}_{Trials}$ (kN)	% Error
10	302.5260	0.3853	43.8088	162.5822	622.0503	647.91	3.99%
11	362.7534	1.5431	53.0087	190.0365	742.5357	763.32	2.72%
12	428.1641	4.9561	63.0847	218.1999	873.9767	898.04	2.68%
13	498.7188	13.4072	74.0369	246.7407	1018.7705	1052.23	3.18%
14	574.3815	31.6381	85.8653	275.3274	1181.2777	1226.01	3.65%
15	655.1194	66.8157	98.5698	303.6283	1368.2887	1419.57	3.61%
16	740.9020	128.7305	112.1506	331.3118	1589.2206	1632.90	2.67%

# **Vortex Generator Drag Reduction Along a Route**

The Vortex Generator Drag Reduction can be applied to the viscous resistance component of the Holtrop-Mennen (1982) approximation, while maintaining constant the other components of resistance, to arrive at the total resistance at full scale (Table 6).

Table 6: Resistance Data with VG Reduction

U (kts)	R <sub>fVG</sub> (kN)	R <sub>Total</sub> (kN)	R <sub>VGReduction</sub> (kN)	VG Reduction
10	278.6009	589.2085	-32.8418	5.42%
11	334.0652	703.1557	-39.3800	5.45%
12	394.3030	827.4958	-46.4809	5.46%
13	459.2778	964.6303	-54.1402	5.46%
14	528.9568	1118.9237	-62.3540	5.42%
15	603.3095	1297.1699	-71.1188	5.34%
16	682.3081	1508.7894	-80.4312	5.19%

The VG reduction applied is from the latest set of experiments at 1.4 m/s where the drag reduction of model scale was 7.9%.

This resistance analysis was also incorporated with the route analysis for the transpacific case, to assess how the VG reduction would perform in an open ocean route. The highest and lowest values of added resistance due to sea state case scenarios, January and July, respectively, were added to the Total Resistance of the vessel both with and without the vortex generator reduction applied to  $R_{\rm f}$  and the net reduction was compared (Tables 7 and 8).

The effective horsepower can also be evaluated:

$$P_{E} = R_{T} U_{s} \tag{3}$$

Table 7: Resistance Data — Trans Pacific Route, January (Worst Case)

U (kts)	R <sub>fVG</sub> (kN)	R <sub>ADDED</sub> (kN)	R <sub>total</sub> (kN)	R <sub>tot VG</sub> (kN)	VG Reduction (kN)	% VGdiff
10	302.5260	175.7813	797.8316	764.9898	32.8418	4.20%
11	362.7534	175.7813	918.3169	878.9370	39.3800	4.38%
12	428.1641	175.7813	1049.7580	1003.2771	46.4809	4.53%
13	498.7188	175.7813	1194.5517	1140.4115	54.1402	4.64%
14	574.3815	175.7813	1357.0590	1294.7050	62.3540	4.70%
15	655.1194	175.7813	1544.0700	1472.9512	71.1188	4.71%
16	740.9020	175.7813	1765.0019	1684.5707	80.4312	4.66%

Table 8: Resistance Data — Trans Pacific Route, July (Best Case)

U (kts)	R <sub>fVG</sub> (kN)	R <sub>ADDED</sub> (kN)	R <sub>TOT</sub> (kN)	R <sub>tot VG</sub> (kN)	VG Reduction (kN)	% VGdiff
10	302.5260	25.625	647.6753	614.8335	32.8418	5.20%
11	362.7534	25.625	768.1607	728.7807	39.3800	5.26%
12	428.1641	25.625	899.6017	853.1208	46.4809	5.30%
13	498.7188	25.625	1044.3955	990.2553	54.1402	5.32%
14	574.3815	25.625	1206.9027	1144.5487	62.3540	5.30%
15	655.1194	25.625	1393.9137	1322.7949	71.1188	5.24%
16	740.9020	25.625	1614.8456	1534.4144	80.4312	5.11%

For the ship equipped with VGs,  $P_E$  at 14 knots (7.20 m/s) is estimated at 17,730 kW, or 23,777 hp. Without VGs,  $P_E$  at 14 knots is 19,253 kW, or 25,818 hp. Using a quasi-propulsive efficiency estimate of 72%, a fuel consumption of 160 g/HP-hr and an average price of \$50/barrel of oil, we arrive at savings of 1,200 barrels of oil per month, or \$120K per month of operation.

# VG EFFECTS ON THE PROPULSIVE EFFICIENCY OF THE SHIP

The reduction of viscous drag and the associated change in the flow streamlines have an impact on the propulsive characteristics of the ship. The wake fraction, w, measures the average velocity defect due to the boundary layer of the ship detaching from the hull; the larger the separation, the larger w is, while non-uniformity of the flow and unsteadiness is introduced. Reducing flow separation causes w to decrease, while unsteady flow effects are reduced as well; the drag reduction is of the order of 7%, so the impact on w will be commensurate. The

thrust deduction factor, t, measures the increase in resistance in a self-propelled hull versus its towing resistance; this increase is caused by the acceleration of the flow at and near the stern of the ship. The effect of VGs is to prevent significant flow separation, causing the rear stagnation point pressure to increase, resulting in a further reduced self-propelled resistance and a correspondingly decrease in t.

As a result, for the design of the propeller, the specific thrust load is reduced, providing for a more efficient propeller. Indeed, in selecting the optimal pitch ratio for a given propeller diameter, D, we employ the quantity  $k_T/J^2$ , where  $k_T=T/(\rho nD^4)$ , T is the propeller thrust,  $J=U_A/(nD)$  (advance ratio), n is the frequency of the propeller, and  $U_A=U(1-w)$  is the average flow speed at the propeller:

Net drag reduction in high block coefficient ships and vehicles using vortex generators

$$k_T/J^2 = \frac{R_T}{\rho U^2 D^2 (1-w)^2 (1-t)} \tag{4}$$

with R<sub>T</sub> denoting the towing resistance at speed U.

Since the effect of the VGs is to reduce RT as shown herein by about 7%, with commensurate reductions of t and w of about 3.5%, it is expected that the value of  $k_T/J^2$  is reduced by up to an estimated 10 %, allowing for a propeller design with higher propeller efficiency.

Equally important, the reduction in the separated turbulent flow when using the VGs, means a reduction in the magnitude of the unsteady loads on the propeller and the rudder. This implies less vibratory loads and stresses and potentially a reduction in cavitation and ventilation effects.

#### **ACKNOWLEDGMENTS**

Financial support by Oldendorff Carriers administered through CBA is gratefully acknowledged. Igor Mogilevsky and Jillian Marie Uzoma contributed valuable material and conducted several experimental tests during the investigation.

#### APPENDIX A

### Scaling the Projected Drag Reduction to Full Scale Ships

We derive the scaling laws that allow us to project the size of VGs and their expected effect at full sale. Let  $\lambda$  represent the ratio of the length of the full scale vessel (L<sub>s</sub>) to the length of the model (L<sub>m</sub>).

$$\lambda = \frac{L_s}{L_m} \tag{5}$$

Since the model is submerged, we do not use Froude scaling, hence we use a separate scaling factor, the ratio of the ship speed to model speed,  $\lambda_U$ :

$$\lambda_U = \frac{U_s}{U_m} \tag{6}$$

The corresponding Reynolds numbers are calculated as follows, using the kinematic viscosity of the fluid (v):

$$Re_s = \frac{U_s \cdot L_s}{\nu} \tag{7}$$

$$Re_m = \frac{U_m \cdot L_m}{\nu} \tag{8}$$

The thickness of the turbulent boundary layer,  $\delta$ , is

SMC 2025, 29-31 October 2025, Norfolk, VA

estimated as:

$$\delta \cong 0.38 \left(\frac{L}{Re^{1/5}}\right) \tag{9}$$

Hence:

$$\delta_s = \delta_m \lambda^{4/5} \lambda_U^{-1/5} \tag{10}$$

Using the International Tow Tank Conference (ITTC, 1957) relation for the frictional coefficient in terms of the Reynolds number at a distance x from the bow, Re(x), we find that the frictional coefficients of the full-scale vessel (Cfs and the model (Cfm) as:

$$C_{fs} \cong \frac{0.0592}{Re_{xs}^{1/5}} \tag{11}$$

$$C_{fs} = \frac{C_{fm}}{\lambda^{1/5} \lambda_U^{1/5}} \tag{12}$$

The scaling factor that determines the VG size is the thickness of the boundary layer at the location of the VGs, viz., 29 mm for model scale and 1.475 m for a ship with length L=300m. Hence, extrapolating from model scale with speed  $U_m=1.3m/s$ , the full-scale VGs have a height of 0.356 m.

In order to estimate the number of VGs for the full scale ship, NV Gm, we use half the circumference of the model (since it is a double hull) and the perimeter of the ship at the location of the VGs, to find at model scale:

$$N_{VGm} = \frac{2\pi r_m^2}{w_{VGm}} \tag{13}$$

where  $r_m$  is the radius of the model, and  $w_{VGm}$  is the width of the VGs at model scale. At full-scale we find:

$$\frac{N_s}{N_m} = \frac{2\pi r_s}{w_s} = \frac{2\pi \lambda r_m}{\lambda^{4/5} \lambda_u^{-1/5}} = \frac{\sqrt[5]{\lambda \lambda_u}}{2}$$
 (14)

Table 9: Model and Full Scale Principal Dimensions

Quantity	Model	Full Scale
Length (m)	1.4	294.4
Speed (m/s)	1.3	7.46
Number of VGs	15	31
Length of VG (m)	0.028	1.424
Width of VG (m)	0.017	0.865
Height of VG (m)	0.007	0.356
Surface Area of VG (m <sup>2</sup> )	0.000298	0.772
$C_{f(ITTC)}$	0.00413	0.01703
Boundary Layer Height (m)	0.029	1.475

Net drag reduction in high block coefficient ships and vehicles using vortex generators

With equations defining the relationships between  $\delta$  and Cf, the net drag reduction ratio can be applied to the full-scale vessel.

The parasitic drag of the model VGs,  $D_{VGm}$  can be found as:

$$D_{VGs} = \frac{1}{2} \rho C_{DVGm} A_{VGm} U_m^2 N_m \tag{15}$$

where  $A_{VGm}$  is the projected area of the VGs, and  $CD_{VGm}$  is the drag coefficient that consists mostly of pressure drag (vortex-making) plus a smaller frictional component. The ratio of the parasitic drag to the viscous drag of the model can be found as:

We can make the conservative assumption that the drag coefficient of the full scale VGs is the same as that of model scale VGs,  $C_{\rm DVGs}$  = $C_{\rm DVGm}$ . It is expected that it will actually be slightly smaller, since the frictional coefficient reduces with Reynolds number, while the dominant, vortex-making part, remains roughly constant. As a result:

$$\frac{D_{VGs}}{D_{fs}} = \frac{A_{VGs}U_s^2 N_s}{A_{VGm}U_m^2 N_m} = (\lambda \lambda_U)^{9/5}$$
 (16)

The viscous drag at the model scale, D<sub>m</sub> is found as:

$$D_m = \frac{1}{2}\rho C_{fm} A_m U_m^2 (1+k) \tag{17}$$

where k is the form factor. We can assume that the form factor is the same at full scale, so that the full-scale drag,  $D_s$  is:

$$D_s = \frac{1}{2}\rho C_{fs} A_s U_s^2 (1+k)$$
 (18)

to arrive at the relation:

$$D_s = D_m (\lambda \lambda_U)^{9/5} \tag{19}$$

Hence, both the viscous drag and the parasitic VG drag (accounting for the fact that there are more VGs at full-scale) scale with the same rate. Since the drag reduction applies to the form drag component, which is equal to k times the viscous drag, and the parasitic drag scales similarly to the viscous drag, we conclude conservatively that the drag reduction at full scale, as a percent of the viscous drag, will be at least equal to the drag reduction at model scale.

### REFERENCES

Achenbach, E. Experiments on the Flow Past Spheres at Very High Reynolds Numbers. Journal of Fluid Mechanics 54, no. 3 (1972): 565–575.

Aguila Ferrandis, J. Net Drag Reduction in Streamlined Bodies with Vortex Generators. PhD thesis, Massachusetts Institute of Technology, 2024.

American Bureau of Shipping. ABS Rules for Building and Classing Marine Vessels: Part 5A and 5B — Specific Vessel Types: Common Structural Rules for Bulk — Carriers and Oil Tankers. Houston, TX: American Bureau of Shipping, January 2025.

Anderson, J. EBOOK: Fundamentals of Aerodynamics (SI Units). McGraw-Hill, 2011.

Babinsky, H., and J. K. Harvey. Shock Wave-Boundary-Layer Interactions, vol. 32. Cambridge: Cambridge University Press, 2011.

Bearman, P. W., and J. K. Harvey. "Golf Ball Aerodynamics." Aeronautical Quarterly 27, no. 2 (1976): 112–122.

Bechert, D. W., M. Bruse, and W. Hage. "Experiments with Three-Dimensional Riblets as an Idealized Model of Shark Skin." Experiments in Fluids 28, no. 5 (2000): 403–412.

Choi, H., W. Jeon, and J. Kim. "Control of Flow over a Bluff Body." Annual Review of Fluid Mechanics 40 (2008): 113–139.

Chowdhury, H., B. Loganathan, Y. Wang, I. Mustary, and F. Alam. "A Study of Dimple Characteristics on Golf Ball Drag." Procedia Engineering 147 (2016): 87–91.

Gad-el Hak, M. Flow Control. Cambridge: Cambridge University Press, 2000. "Flow Control: The Future." Journal of Aircraft 38, no. 3 (2001): 402–418.

Godard, G., and M. Stanislas. "Control of a Decelerating Boundary Layer. Part 1: Optimization of Passive Vortex Generators." Aerospace Science and Technology 10, no. 3 (2006): 181–191.

Hama, F. R., J. D. Long, and J. C. Hegarty. "On Transition from Laminar to Turbulent Flow." Journal of Applied Physics 28, no. 4 (1957): 388–394.

Holtrop, Jan, and G. G. J. Mennen. "An Approximate Power Prediction Method." International Shipbuilding Progress 29, no. 335 (1982): 166–170.

International Towing Tank Conference (ITTC). Recommended Procedures and Guidelines: Performance, Power, and Propulsion — The 1957 ITTC Line. Technical Report ITTC-1957. Standard method for extrapolation of model ship resistance data, 1957.

Jirasek, A. "Vortex-Generator Model and Its Application to Flow Control." Journal of Aircraft 42, no. 6 (2005): 1486–1491.

Johnston, J. P., and M. Nishi. "Vortex Generator Jets—Means for Flow Separation Control." AIAA Journal 28, no. 6 (1990): 989–994.

Kimmeth, J. "Wedged Vortex Generator Applications for Marine Vessels." Master's thesis, Massachusetts Institute of Technology, 2025.

Kuethe, A. M. "Boundary Layer Control of Flow Separation and Heat Exchange." U.S. Patent 3,741,285, 1970.

Larsson, L. Ship Resistance and Flow. The Principles of Naval Architecture Series. New York: The Society of Naval Architects and Marine Engineers (SNAME), 2010.

Li, X., W. Liu, T. Zhang, P. Wang, and X. Wang. "Analysis of the Effect of Vortex Generator Spacing on Boundary Layer Flow Separation Control." Applied Sciences 9, no. 24 (2019): Article 5495.

Li, X., K. Yang, and X. Wang. "Experimental and Numerical Analysis of the Effect of Vortex Generator Height on Vortex Characteristics and Airfoil Aerodynamic Performance." Energies 12, no. 5 (2019): Article 959.

Lin, J., H. Floyd, D. S. Bushnell, and G. Selby. Investigation of Several Passive and Active Methods for Turbulent Flow Separation Control. Aerospace Research Center Report, 1990, p. 1598.

Lin, J. C. "Review of Research on Low-Profile Vortex Generators to Control Boundary-Layer Separation." Progress in Aerospace Sciences 38, no. 4–5 (2002): 389–420.

Mogilevsky, I. Shipping Decarbonization through Sea Route Optimization & Vortex Generator Resistance Reduction. Master's thesis, Massachusetts Institute of Technology, 2022. Mohseni, K. "Pulsatile Vortex Generators for Low-Speed Maneuvering of Small Underwater Vehicles." Ocean Engineering 33, no. 16 (2006): 2209–2223.

Molland, A. F., S. R. Turnock, and D. A. Hudson. Ship Resistance and Propulsion. Cambridge: Cambridge University Press, 2011.

Murai, Y., H. Sakamaki, I. Kumagai, H. J. Park, and Y. Tasaka. "Mechanism and Performance of a Hydrofoil Bubble Generator Utilized for Bubbly Drag Reduction Ships." Ocean Engineering 216 (2020): Article 108085.

Oledal, M. "Application of Vortex Generators in Ship Propulsion System Design." WIT Transactions on the Built Environment 27 (1970).

Rostamzadeh-Renani, M., R. Rostamzadeh-Renani, M. Baghoolizadeh, and N. K. Azarkhavarani. "The Effect of Vortex Generators on the Hydrodynamic Performance of a Submarine at a High Angle of Attack Using a Multi-Objective Optimization and Computational Fluid Dynamics." Ocean Engineering 282 (2023): Article 114932.

Saric, W. S., H. L. Reed, and E. J. Kerschen. "Boundary-Layer Receptivity to Freestream Disturbances." Annual Review of Fluid Mechanics 34, no. 1 (2002): 291–319.

Schlichting, H., and J. Kestin. Boundary Layer Theory, vol. 121. New York: Springer, 1961.

Schubauer, G. B., and H. K. Skramstad. "Laminar Boundary-Layer Oscillations and Transition On." Journal of Research of the National Bureau of Standards 38 (1947): 251.

Schubauer, G. B., and W. G. Spangenberg. "Forced Mixing in Boundary Layers." Journal of Fluid Mechanics 8, no. 1 (1960): 10–32.

Simpson, R. L. "Turbulent Boundary-Layer Separation." Annual Review of Fluid Mechanics 21, no. 1 (1989): 205–232.

Smith, A. Milton O. Transition, Pressure Gradient and Stability Theory. Technical report, Douglas Aircraft Co., 1956.

Stephens, A. V., and E. Bay. "Solid Boundary Surface for Contact with a Relatively Moving Fluid Medium." U.S. Patent 2,800,291, 1957.

U.S. Government Publishing Office. Code of Federal Regulations: Title 46, Part 92, Subpart 92.01 — Structure. CFR, Title 46, Chapter I, Subchapter I, 2024. Revised as of October 1, 2024.

Wheeler, G. O. "Means of Maintaining Attached Flow of a Flow Medium." U.S. Patent 4,455,045, 1984. "Low Drag Vortex Generators." U.S. Patent 5,058,837, 1991.